Journal of Analytical and Applied Pyrolysis 120 (2016) 186–193

Contents lists available at ScienceDirect

Journal of Analytical and Applied Pyrolysis

journal homepage: www.elsevier.com/locate/jaap

Biomass pyrolysis for nitrogen-containing liquid chemicals and nitrogen-doped carbon materials

Wei Chen, Haiping Yang, Yingquan Chen*, Xu Chen, Yang Fang, Hanping Chen

State Key Laboratory of Coal Combustion, Huazhong University of Science and Technology, 1037 Luoyu Road, 430074 Wuhan, PR China

ARTICLE INFO

Article history:
Received 19 November 2015
Accepted 4 May 2016
Available online 5 May 2016

Keywords:
Biomass
Nitrogen-enriched pyrolysis
Nitrogen-containing chemicals
Nitrogen-doped bio-char

ABSTRACT

A novel biomass pyrolysis technique was proposed that introduced exogenous nitrogen for the production of nitrogen-containing chemicals and nitrogen-doped bio-char materials. The influence of NH_3 and KOH addition on bamboo pyrolysis was investigated using micro-gas chromatography, gas chromatography–mass spectroscopy, accelerated surface area and porosimetry, X-ray photoelectron spectroscopy and electrochemical analysis. The introduction of NH_3 slightly increased bio-oil yield and the production of nitrogen-containing species at the expense of phenols and aromatics. Specific surface area, overall nitrogen content and the number of nitrogen-containing functional groups of the solid bio-char also increased significantly, while H_2 content of the evolved gas spiked significantly. Meanwhile, the addition of KOH increased bio-char yield with an increased in specific surface area up to 1873 $m^2\ g^{-1}$. Furthermore, the specific capacitance of the bio-char electrodes reached to 187 $F\ g^{-1}$, indicating excellent capacitive performance. Results showed biomass nitrogen-enriched pyrolysis was a promising method for more efficient utilization of biomass resources.

1. Introduction

Biomass is a clean, renewable and abundant resource that can be converted to bio-char, bio-oil and fuel gas through various thermochemical processes [1,2]. Conversion of biomass for high value products is an important development direction for biomass utilization, which has attracted more attention [3,4]. Most notably, biomass pyrolysis can produce both nitrogen-containing compounds and nitrogen-doped bio-char [5,6]. Nitrogen-containing compounds like pyrrole, pyridine, indol and their derivatives can be used to produce pharmaceuticals, dyes, perfumes and other commercial products [6,7]. Meanwhile, nitrogen-doped carbon materials can be used in catalysis, CO_2 adsorption and electrode materials for supercapacitors and batteries [8–10].

Ferrera-Lorenzo et al. [11] found high pyrrole and pyridine content in the bio-oil product from macroalgae waste pyrolysis. Likewise, Marcilla et al. [6] determined that pyrrole and pyridine derivates (2,2,6,6-tetramethyl-1,4-piperidinone and 6-methyl-2,2′-bipyridine-1-oxide) were the highest yielding compounds in the liquid oil resulting from tannery waste pyrolysis. In addition, Wang et al. [12] prepared biomass-based activated carbons with high nitrogen content from willow catkins; the resulting material showed high specific capacitance. Furthermore, Li et al. [9] synthesized excellent carbon electrode materials for supercapacitor with 8% nitrogen derived from chicken eggshell membranes.

However, the nitrogen content of most agricultural and forestry waste is quite low, consequently the yield and quality of nitrogen-containing products is very limited [13]. Hence, it is necessary to optimize any processing procedures and, frequently, to introduce exogenous nitrogen, often accomplished using NH_3, urea, melamine or aniline, among others. For example, Xu et al. [14] reported that bio-derived furans could be converted to indoles directly by treating them with NH_3 over acidic catalysts. In addition, Zhou et al. [15] prepared nitrogen-doped porous carbons materials with good capacitance characteristics from the pyrolysis of polymerized ethylenediamine and carbon tetrachloride. Furthermore, Sun et al. [16] synthesized nitrogen-enriched carbon materials by the co-pyrolysis of tetraethyl orthosilicate, nickel nitrate, glucose and melamine; again, the resulting materials showed excellent capacitive behavior. However, all previous work has concerned only the production of a single product from model compounds or biomass derivatives; there are no reports of the overall pyrolysis, including procedural information and product characterization, of a biomass after the addition of exogenous nitrogen.

This study analyses the effects of NH_3, as an exogenous nitrogen source, on bamboo pyrolysis. Both the overall process and the

* Corresponding author.
E-mail addresses: chenwei_hk@163.com (W. Chen), yhping2002@163.com (H. Yang), chyq721@163.com (Y. Chen), cxu200911594@163.com (X. Chen), fyy912@126.com (Y. Fang), hp.chen@163.com (H. Chen).

http://dx.doi.org/10.1016/j.jaap.2016.05.004
0165-2370/

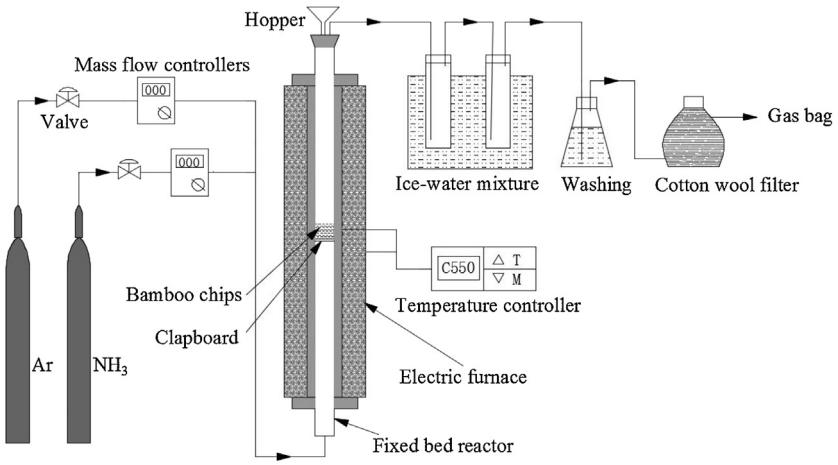

Fig. 1. The fixed bed nitrogen-enriched pyrolysis system.

Table 1
Compositions and low heating value of gas product from bamboo pyrolysis (vol.%).

Compositions	BC	BC-N	BC-0.1-N	BC-0.2-N	BC-0.3-N	BC-0.4-N
H_2	15.6	38.0	57.9	55.9	55.4	53.4
CH_4	17.9	13.7	6.6	6.5	6.0	6.0
CO	44.7	32.7	17.4	22.1	23.6	26.9
CO_2	17.5	9.1	8.0	8.2	8.2	8.0
C_2H_4	3.3	2.2	1.0	1.1	1.1	1.1
C_2H_6	1.0	0.8	0.5	0.7	0.7	0.7
N_2	–	3.5	8.6	5.5	5.0	3.9
LHV (MJ Nm^{-3})	16.62	15.67	12.96	13.06	12.96	13.03

products were reviewed in detail. Furthermore, the influence of KOH was assessed, as it is a commonly used activator for increasing the specific surface area and porosity of nitrogen-doped bio-char [17–19]. And the mechanism of migration and transformation of nitrogen in the products was explored. The results will be helpful for realizing more efficient utilization of biomass resources.

2. Methods

2.1. Samples

Bamboo chips were obtained locally. They were dried at 105 °C for 24 h, crushed and sieved to yield bamboo particles 0.25–0.6 mm in size. Detailed information about the bamboo chips is presented in Table S1.

KOH (≥99.5, AR) was obtained from Sinopharm Chemical Reagent. Bamboo chips samples were treated with KOH solution at KOH/bamboo chips weight ratios of 0.1, 0.2, 0.3 and 0.4 (solution-to-feedstock was 15 mL g^{-1}); these samples were named BC-0.1, BC-0.2, BC-0.3 and BC-0.4, respectively. After treatment, water was evaporated by heating the samples at 60 °C under stirring with nitrogen.

2.2. Pyrolysis experiment

Fast pyrolysis of bamboo chips was carried out in a fixed bed system, as shown in Fig. 1. The system included a fixed bed reactor (1000 mm height, 45 mm inner diameter), electric furnace, temperature controller, condensing system, gas cleaning and drying system.

For each trial, the reactor was first heated to a preset temperature 800 °C under a flow of 500 mL min^{-1} Ar (99.99%), after which 50 mL min^{-1} NH_3 (99.99%) was introduced as Ar flow rate was decreased to 450 mL min^{-1}. When the system reached the steady state, the sample (~2 g) was promptly fed into the reactor and retained for 60 min. Bamboo particles were heated up, and the volatiles evolved out quickly. The condensable volatiles were collected in the condensing system using an ice-water mixture, while the non-condensable components were cleaned by the washing bottle with water solution. Gas product was filtered and dried in a cotton wool filter with silica gel, after which they were collected with a gas bag for further analysis.

After pyrolysis experiment, the reactor was cooled to ambient temperature under a flow of 500 mL min^{-1} Ar. The bio-char, bio-oil and gas were collected. Bio-char yield was calculated by weighing the solid sample, while bio-oil yield was obtained by measuring the mass difference of the condensing system. Likewise, gas yield was measured by combing the volumes of the gas products collected during the pyrolysis process. The bio-oil in the condenser system, which could be collected directly with good fluidity, was named the aqueous phase, while the bio-oil, condensed in the gas-line tube and collected with acetone, was named the non-aqueous phase. Each experiment was performed three times with good repeatability (5 relative standard deviation (RSD)%), after which the data took the average.

All the resultant bio-chars were immersed with 1 M HCl to remove potassium contained compounds, and subsequently washed with deionized water until the pH value of the filtrate was approximately 7. They were then dried in an electrical oven at 105 °C for 24 h. The samples pyrolysis with a mixture of Ar and NH_3 were named BC-N, BC-0.1-N, BC-0.2-N, BC-0.3-N and BC-0.4-N with respect to the names of the samples prior to treatment. As a comparison, an untreated sample was pyrolyzed at 800 °C with pure Ar (500 mL min^{-1}) and was named BC.

2.3. Measurement of gas and bio-oil

A dual-channel micro-gas chromatography system (Micro-GC 3000A, Agilent Technologies, USA) with thermal conductivity detectors was used to analyse the gaseous products quantitatively. The detailed analytical method has been described elsewhere [20]. The low heating value (LHV) of the gas products can be calculated as follows [21]:

$$\mathrm{LHV(MJ\,Nm^{-3})} = 0.126 \times \mathrm{CO} + 0.108 \times \mathrm{H_2} + 0.358 \times \mathrm{CH_4} + 0.665 \times \mathrm{C_nH_m} \quad (1)$$

where CO, H_2, CH_4 and C_nH_m ($C_nH_m = C_2H_2 + C_2H_4 + C_2H_6$) are the volume fractions of those species.

Table 2
Classification of aqueous phase and non-aqueous phase (% of total peak area).

Classifications	BC	BC-N	BC-0.1-N	BC-0.2-N	BC-0.3-N	BC-0.4-N
Aqueous phase						
N compounds	2.3	58.0	49.7	46.1	53.9	53.6
N/O compounds	–	28.9	29.6	40.5	25.3	37.3
O compounds	24.3	4.1	4.7	4.7	8.1	3.7
phenols	73.4	–	–	–	–	–
Non-aqueous phase						
N compounds	2.8	27.5	30.3	22.8	61.4	14.9
N/O compounds	–	28.7	6.6	22.6	7.1	18.8
O compounds	5.1	11.0	9.4	8.6	6.3	10.8
aromatics	25.3	3.0	10.0	4.7	3.8	15.2
phenols	38.7	11.1	29.9	21.4	5.4	25.8

*(i) N compounds, compounds in which the only heteroatom is N; (ii) N/O compounds, compounds in which both N and O are present; (iii) O compounds, compounds in which the only heteroatom is O (excluding phenols).

The nitrogen-containing gas component was measured with a Gasmet Dx-4000 Fourier transform infrared spectroscopy (FTIR) multicomponent gas analyzer (Temet Instruments OY, Finland) [22,23]. This device included a FTIR spectrometer, a temperature-controlled sample cell and signal processing electronics. The transfer line and the gas cell were kept at 180 °C to avoid condensation or adsorption of semivolatile products.

The main chemical species of the bio-oil were identified using gas chromatography–mass spectroscopy (GC-MS, HP7890 series GC with an HP5975 MS detector) with a capillary column (Agilent: HP-5MD, 19091s-433; 30 m × 0.25 mm i.d. × 0.25 μm d.f.). The GC1034C Chemstation, with a National Bureau of Standards library (NIST2011), was used to identify each compound based on the retention time and the matching mass spectrum of the standards in the spectral library. The analytical method used here is detailed in our previous study [2].

The water content of the bio-oil was measured using a Karl-Fischer titration (TitroLine KF-10, Schott, Germany). The pH value of the bio-oil was determined using an Ohaus electrode.

2.4. Characterization of bio-char

Solid char composition was determined through ultimate analysis using a CHNS/O elementary analyser (Vario Micro Cube, Germany). Proximate analysis were measured following the American Society for Testing and Materials standards to obtain the moisture, volatile, fixed carbon and ash content. The LHV of the bamboo chips was measured using bomb calorimetry (Parr 6300, USA).

The porous characteristics of bio-char were measured using nitrogen isothermal adsorption at 77 K with an accelerated surface area and porosimetry system (ASAP 2020, Micromeritics, USA). The CO_2 adsorption isotherm at 273 K was obtained at relative pressures (P/P_0) ranging from 10^{-6} to 0.3, in order to calculate narrow micropore structure. Prior to the adsorption, the samples were degassed at 150 °C for 10 h. BET specific surface area (S_{BET}) was determined by the Brunauer-Emmett-Teller (BET) equation. Micropore surface area (S_{mic}) and Micropore volume (V_{mic}) were determined by *t*-plot method. The total pore volume (V_{total}) was determined by single point adsorption total pore volume analysis. Average pore diameter (D) was determined by $4V/S_{BET}$ based on BET method. The narrow micropore surface area ($S_{n\text{-}mic}$) and narrow micropore volume ($V_{n\text{-}mic}$) were obtained by Dubinin-Astakhov (DA) method. The pore size distribution plot was obtained by the density function theory method.

The nitrogen-containing functional groups on the surface of bio-char were analysed with X-ray photoelectron spectroscopy (XPS, Axis Ultra DLD, Kratos, UK) using Al Kα line (15 kV, 10 mA, 150 W) as a radiation source. C1*s* peak position, set at 285 eV, was used as an internal standard. The curves on N1*s* peaks were fitted by XPS-peak4.1 software. The content of each element was determined by the corresponding peak area and calibrated by the atomic sensitivity factor with C as reference.

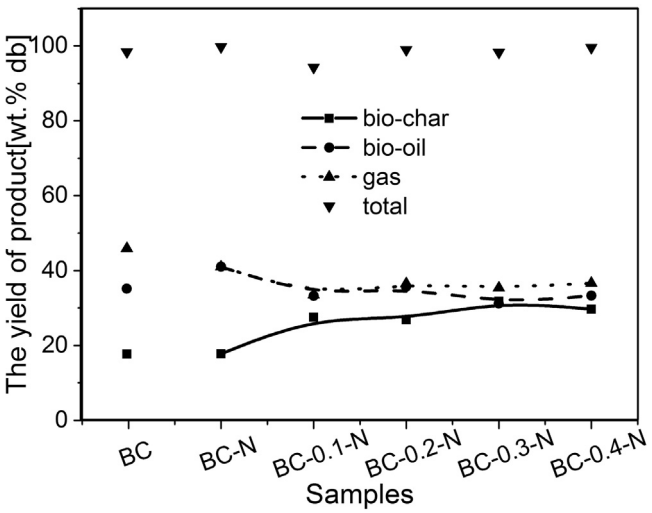

Fig. 2. The products distribution of different samples pyrolysis.

The electrochemical property of bio-char was measured in a three-electrode system with an electrolyte of 6 M KOH using a CHI760 (CH Instruments, USA) electrochemical workstation at ambient temperature. A Platinum plate and saturated calomel electrode were used as the counter and reference electrode, respectively. The working electrode was prepared as follows: The bio-char (80%) with acetylene black (10%) and poly(vinylidene fluoride) (PVDF, 10%) were mixed uniformly and dispersed in *N*-methyl-2-pyrrolidone (NMP) to form the slurry. Then the slurry was coated onto a 1 cm × 1 cm nickel foam current collector, and dried at 110 °C for 12 h in the vacuum oven. Finally, it was pressed at a pressure of 10 MPa, and the mass difference was obtained to calculate the mass of the bio-char on the working electrode. The cyclic voltammetry (CV) was performed at different scan rates. The galvanostatic charge/discharge (GCD) properties were carried out at different current densities. The electrochemical impedance spectroscopy (EIS) measurements were performed at frequencies from 0.01 Hz to 100 kHz in a voltage amplitude of 5 mV.

3. Results and discussion

3.1. Property of bamboo pyrolysis

The bio-char, bio-oil and gas product yields of variant samples pyrolysis are shown in Fig. 2. Solid char yield was quite low (~17.5 wt.%) for pure Ar, while gas and liquid oil yields were very high, at about 45.8 and 36.7 wt.%, respectively. This was due to the high volatile content and high pyrolysis temperature [24,25]. When NH_3 was added, the gas yield decreased greatly while the bio-oil yield increased accordingly, however, no obvious change was observed for the bio-char yield. The addition of KOH increased the yield of bio-char significantly and with respect to the amount of KOH used, an effect that was in part due to the excess KOH remaining after pyrolysis; the bio-oil content did decrease, though more gradually than the increase in bio-char content, while no obvious effects were observed for gas yield, which kept constant at around 36 wt.%.

3.2. The releasing property of pyrolysis gas

Table 1 shows the properties of gas products from bamboo pyrolysis. Pure Ar gave a gas mainly consisted of CO with some CH_4, H_2, CO_2 and trace C_2H_4 and C_2H_6. The LHV was slightly over 16 MJ Nm^{-3}, which corresponded to medium heat value gas fuel that can be used in industrial boilers [26]. Adding NH_3 increased the H_2 content drastically, to 38.0 vol.%, while CO, CO_2 and CH_4 content decreased accordingly. This suggested that NH_3 reacted with biomass at high temperature, generating H atoms and the corresponding NH_2 and NH radicals; merger of the H atoms would have then led to the increase in H_2. A possible pathway of H_2 generated can be described as follows [27,28]:

$$(C)_{biomass} + NH_3 \rightarrow C^* + H^* + NH^* + NH_2^* \rightarrow H_2 + C-NH + C-NH_2 \quad (2)$$

In addition, NH_3, NH_2^* and NH^* can react with carbonyl groups through Maillard reaction [29], suppressing decarbonylation and decarboxylation and inhibiting CO and CO_2 formation.

The addition of KOH increased H_2 content significantly and largely decreased CO, CO_2, CH_4, C_2H_4 and C_2H_6 content. This could be the result of reaction between KOH and carbons to form H_2, K_2CO_3 and some K metal during biomass pyrolysis process listed as follows [30–32]:

$$6KOH + 2C \leftrightarrow 2K + 3H_2 + 2K_2CO_3 \quad (3)$$

As KOH content increased, H_2 content decreased slightly and CO concentration increased, with no obvious change for the other gases. Combining the effects of both KOH and NH_3 gave the highest observed H_2 content of 57.9 vol.%; only 17.4 vol.% CO was observed at a KOH/bamboo chips weight ratio of 0.1. In addition, the addition of NH_3 and KOH decreased the LHV of gas product, while the effect of concentration of KOH was fairly small. The gas product of nitrogen-rich pyrolysis still gave relatively high LHV of about 13 MJ Nm^{-3}.

Furthermore, N_2 was detected in the gas products of pyrolysis using NH_3 at fairly high concentrations of 3.5–8.6 vol.%; this might be the bio-char catalyzed reduction of NO, in turn produced from the reaction of NH_3 with biomass [33]; And part of NO could be reduced by NH_3 to form N_2 with char as the catalyst [34]; NH_3 also could have been decomposed catalytically directly to N_2 and H_2 in the presence of bio-char. Overall N_2 content decreased as the KOH/bamboo chips ratio increased.

Importantly, NH_3 was not detected during multicomponent gas analyzer, meaning that it was completely removed during washing. Furthermore, no NO_2, NO, N_2O or HCN were detected, meaning that the gas products can be used as high quality fuel without the problem of nitrogen contained pollution.

3.3. Property of the nitrogen-containing bio-oil

Aqueous phase bio-oil products accounted for 90–93 wt.% of all obtained bio-oils. This phase was yellow and non-viscous. In fact, the aqueous product from bamboo pyrolysis without NH_3 and KOH was nearly colorless. The moisture content of the aqueous phase was quite high, at 52–62 wt.%. However, the non-aqueous phase was black and extremely viscous, simultaneously, the water content was undetectable.

The typical chemical compositions of aqueous and non-aqueous phase are listed in Tables S2 and S3 (see the Supplementary materials, to simply the data processing and analyzing, the compounds with peak area less than 1% and quality matches below 60% were not included). The total percentage of GC–MS area showed here around 72–100%. The main organics in the aqueous phase (Table S2) for pure Ar pyrolysis were acetic acid, phenol and *p*-cresol. However, with the introduction of NH_3, acetic acid was diminishing, which might be due to the acid-base neutralization reaction between NH_3 and acetic acid volatile; indeed, the aqueous phase was weakly alkaline, with a pH of about 9. This loss of acidity is an added benefit with respect to downstream utilization.

Table 3
Porous characteristics of bio-char.

Samples	S_{BET} ($m^2\ g^{-1}$)	S_{mic} ($m^2\ g^{-1}$)	V_{total} ($cm^3\ g^{-1}$)	V_{mic} ($cm^3\ g^{-1}$)	D (nm)
BC	158	148	0.075	0.069	1.898
BC-N	521	470	0.248	0.219	1.902
BC-0.1-N	774	693	0.367	0.323	1.897
BC-0.2-N	1205	1039	0.573	0.481	1.901
BC-0.3-N	1522	1032	0.735	0.477	1.932
BC-0.4-N	1873	522	0.939	0.219	2.006

Moreover, NH_3 addition resulted in the formation of nitrogen-containing compounds, specifically 1-(dimethylamino)-2-butanol, *N*-(1-methylpropylidene)-2-propanamine and 2,2,6,6-tetramethyl-4-piperidinone [6]. Again, these compounds might have resulted from the reaction of NH_3, NH_2^* and NH^* with carbonyl groups and formed the nitrogen-containing functional groups (such as —CH(OH)—NH_2, —CH(OH)—NH—, —CH=NH, —CH=N— etc.), then they might occur the dehydration or condensation reaction and formed heterocyclic nitrogen compounds [35] and the other nitrogen-containing compounds. However, the detailed formation mechanism is still unclear and will need to be investigated in the future. Meanwhile, the addition of KOH replaced 1-(dimethylamino)-2-butanol with 4-amino-4-methyl-2-pentanone [7] as the main nitrogen-containing compounds. There was no clear correlation between KOH concentration and the composition of the nitrogen-containing compounds, although the listed compounds were still the highest yielding in each trial.

The main species in the non-aqueous phase (Table S3) for pure Ar pyrolysis were phenol, *p*-cresol and 4-vinyl phenol. The addition of NH_3 and KOH gave compositions and pH that were similar to the aqueous phase, although they were admittedly more complex.

The two phases are classified [6] in Table 2. Phenols were the major component of the aqueous phase for pure Ar pyrolysis, at 73.4%. However, the addition of NH_3 changed this significantly, with N and N/O compounds accounting for 79–91%. Alternatively, phenols and aromatics together accounted for just 64.1% of the non-aqueous phase derived from pure Ar pyrolysis. The addition of NH_3 increased significantly O compounds, aromatics and phenols yields. However, N and N/O compounds were still the major components, at 34–69%. As seen previously, there was no clear correlation between phase composition and extent of KOH addition.

3.4. Physical and chemical property of the nitrogen-doped bio-char

The porous properties of the different bio-chars are listed in Table 3. The bio-char produced using pure Ar showed lower S_{BET}, with a value of 158 $m^2\ g^{-1}$. BC-N, meanwhile, showed a significantly increased S_{BET} and V_{total} of 521 $m^2\ g^{-1}$ and 0.248 $cm^3\ g^{-1}$, respectively. This is consistent with Reaction (3), in that the H^*, NH_2^* and NH^* can etch carbon fragments and significantly open the material pores through the formation of nitrogen-containing functional groups [27,28,36].

KOH addition, meanwhile, gave even greater increases in S_{BET} and V_{total}, with values of 774 $m^2\ g^{-1}$ and 0.367 $cm^3\ g^{-1}$, respectively, for BC-0.1-N. This effect became more pronounced as KOH concentration increased, with corresponding values of 1873 $m^2\ g^{-1}$ and 0.939 $cm^3\ g^{-1}$, respectively, for BC-0.4-N. This is consistent with Reaction (3), which demonstrates the possible formation of K metal. This metal has a boiling point of 762 °C; as such, it is possible that some of the material is removed from the carbon matrix, while the rest is intercalated, which produces the pore opening to generate the micropores and mesopores [31]. Furthermore, as the

Table 4
Result of elemental and XPS analysis and specific capacitance of bio-char.

Samples	Elemental analysis/wt.%		XPS/atomic %			N 1*s*/area %				$C_{spec}/(F\,g^{-1})$
	C_{daf}	N_{daf}	C	N	O	N-1	N-2	N-3	N-4	
BC	80.6	0.8	95.0	0.3	4.7	–	–	–	–	–
BC-N	90.6	7.3	92.1	4.0	3.9	37.7	25.6	27.6	9.1	39
BC-0.1-N	83.2	10.4	89.7	6.4	3.9	35.1	33.1	10.7	21.0	133
BC-0.2-N	89.3	9.6	90.9	6.3	2.8	32.7	32.4	8.2	26.7	146
BC-0.3-N	75.9	9.6	90.6	6.6	2.8	32.5	40.3	12.8	14.4	161
BC-0.4-N	70.5	9.1	90.5	7.0	2.5	36.0	37.2	9.5	17.3	187

daf: dry ash-free basis.

K metal can be swept out by carrier gas Ar, more K metal will be evaporated out to make the reaction equilibrium. It can increase the reactivity between KOH and bamboo chips further [37].

On the other hand, S_{mic} and V_{mic} initially increased with the addition of KOH, though this effect reversed itself as the KOH/bamboo chips weight ratio increased above 0.2. This indicates that more mesopores were formed and it was consistent with the changing trend of average pore diameter.

The narrow micropore characteristics of the bio-char, as determined by CO_2 adsorption, are shown in Table S4. The narrow micropore surface area ($S_{n\text{-}mic}$) and narrow micropore volume ($V_{n\text{-}mic}$) increased dramatically with NH_3 and KOH introduced in. $S_{n\text{-}mic}$ and $V_{n\text{-}mic}$ increased to 2198 $m^2\,g^{-1}$ and 0.778 $m^3\,g^{-1}$, respectively, at KOH/bamboo chips weight ratio of 0.4.

Fig. 3a shows the pore size distribution curves of the different bio-chars. The addition of NH_3 resulted in a significant increase of the pore volume at the pore diameter of 2.0–2.7 nm. KOH addition gave an initial increase of the pore volume at the pore diameter of ~2 nm, though this value increased with concentration, yielding many pores with 2–3 nm diameters for KOH/bamboo chips ratios over 0.3. The continual increase of the pores with 2–4 nm diameters resulted in mesopores becoming dominant over micropores, accounting for 70% of all pores in the sample at the highest ratio. This coexistence of micropores and mesopores is believed to be ideal for supercapacitors, which can be ascribed to the actual energy storage occurring predominately in the micropores, while the mesopores provide fast mass-transport of electrolytes to and from the micropores [38]. Fig. 3b shows that most narrow micropores of different samples have pore diameters of 0.45–0.65 and 0.75–0.8 nm. The addition of NH_3 significantly increased the pore volume for diameters of 0.5–0.6 nm. The same effect occurs with KOH addition for diameters of 0.55–0.65 and 0.75–0.8 nm.

Fig. 4a shows the cyclic voltammetry curves of solid bio-chars. It could be observed that the CV curve of BC deviated from rectangular shape seriously, indicating the bad capacitive behavior due to its low specific surface area. The addition of NH_3 caused the CV curve of BC-N to deviate a little from rectangular shape without obvious redox peaks, as the specific surface area was not big enough with low nitrogen content. Adding KOH resulted in the CV curves presenting the rectangular-like shapes with a couple of redox peaks at around −0.8 V, indicating the co-existence of the good electrical double-layer capacitance behavior and pseudo-capacitive phenomena of the nitrogen-doped bio-char electrodes.

Fig. 4b shows the galvanostatic charge/discharge curves of different samples. Adding KOH resulted in a little deviation from linear characteristics of the GVD curves, which was due to the pseudo-capacitive behavior of the nitrogen-containing bio-char electrodes. However, the deviations of GCD curves of BC and BC-N from the triangle shape (especially BC, its specific capacitance was not calculated due to the bad capacitive behavior) were due to the undesirable capacitive behavior. These results were consistent with the CV curves analyses. The specific capacitance of bio-char electrode materials were calculated according to their GCD curves

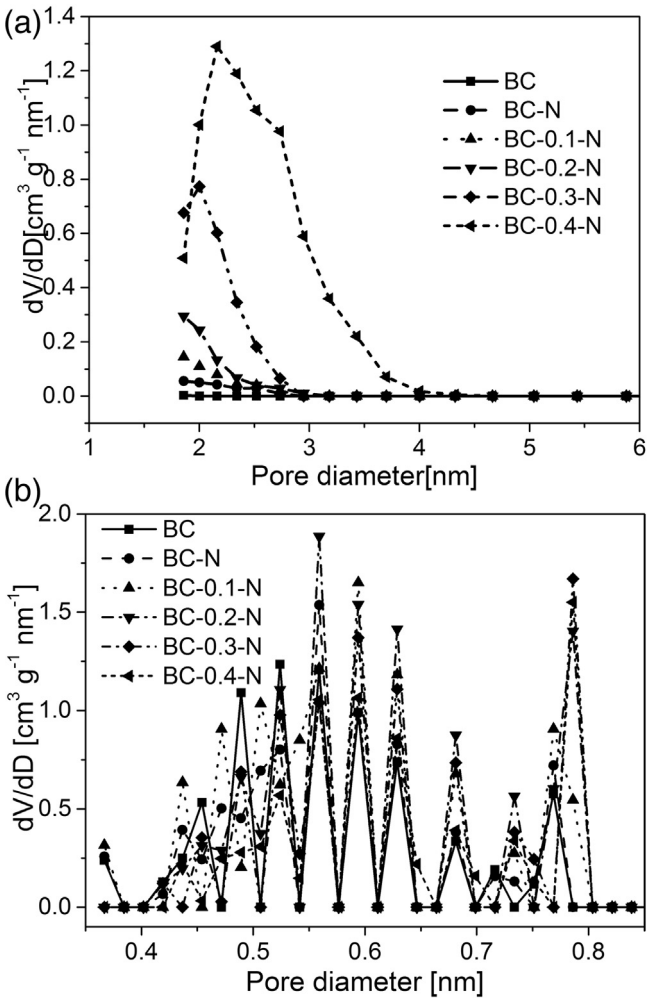

Fig. 3. Pore size distribution curves of different samples by N_2 (a) and CO_2 adsorption (b).

[16,39] and is listed in Table 4. C_{spec} increased significantly with KOH addition, likely due to both an increase in nitrogen content on the surface as well the discussed increase in S_{BET}. A maximum value of 187 $F\,g^{-1}$ was observed for a KOH/bamboo chips weight ratio of 0.4. In addition, the current increased when enhancing the scan rate, revealing its good rate capability (Fig. S1a). The GCD curves presented the triangle shape, demonstrating the charge/discharge reversibility (Fig. S1b). C_{spec} still retained 85% after 3000 GCD cycles at 1 $A\,g^{-1}$, indicating excellent reversibility and stability (Fig. S1c).

Fig. 4c illustrates the Nyquist plots of different bio-char samples. The Nyquist plot composed of three sections: (1) at low frequency, the curve were nearly a vertical line, characterizing the electrical double-layer capacitance behavior, (2) at intermediate frequency, a nearly 45° diagonal line (Warburg region) was observed, indi-

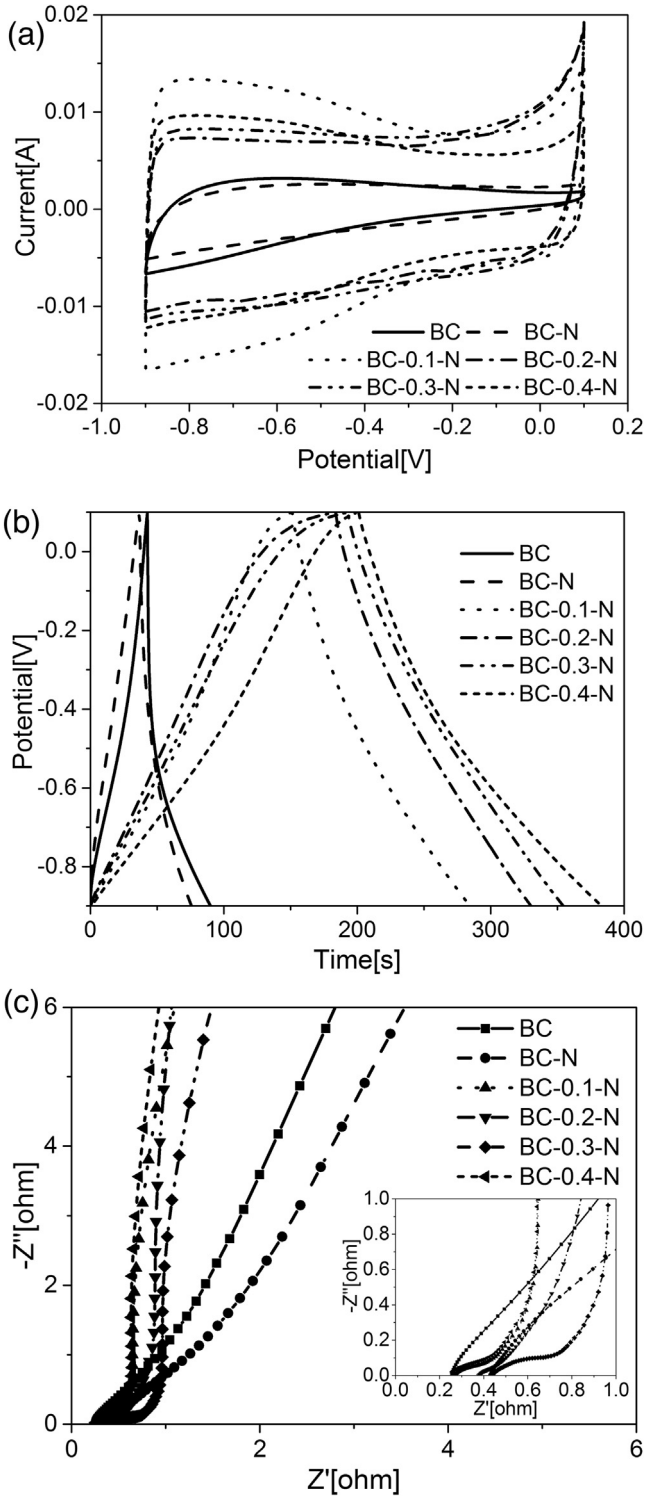

Fig. 4. Electrochemical performance of bio-chars: (a) Cyclic voltammetry curves at 10 mV s^{-1}; (b) Galvanostatic charge/discharge curves at 1 A g^{-1}; (c) Nyquist plots (the inset shows the expanded high frequency region of the plot).

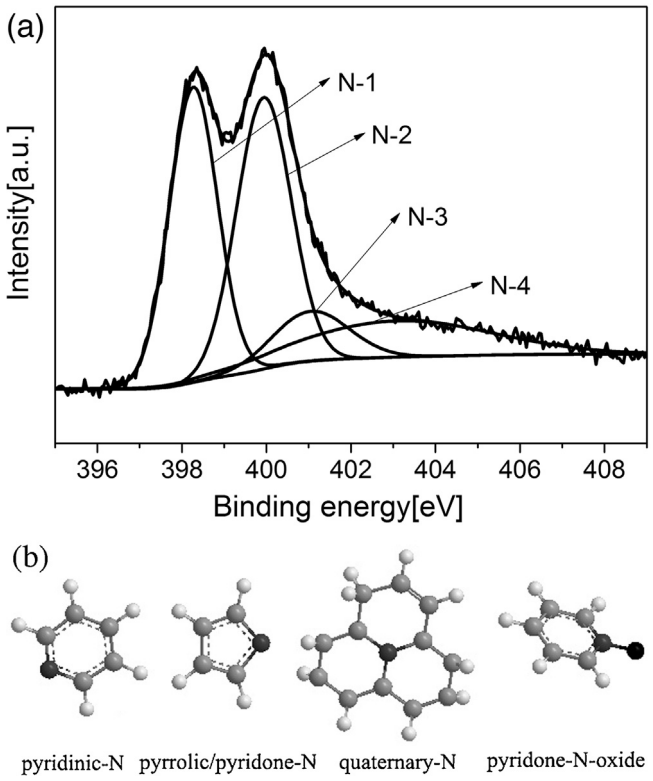

Fig. 5. XPS spectra of BC-0.4-N (a) and chemical structure of four nitrogen-containing functional groups (b).

cating the ion diffusive resistance within the electrode materials, (3) at high frequency, a semicircle implied the charge transfer resistance [40,41]. The addition of KOH gave more vertical lines, showing the better electrical double-layer capacitance characteristics at low frequency. In addition, no obvious semicircle was observed at high frequency for all electrode materials, demonstrating the low charge transfer resistance [42]. The values of the equivalent series resistance (ESR) of all the electrodes were relatively low (<0.5 Ω), revealing the good conductivity of the electrode materials.

The elemental composition of the solid char is listed in Table 4. The introduction of NH_3 significantly increased nitrogen content in the bio-char, while the oxygen content on the surface of bio-char decreased obviously due to the preferential reaction between NH_3 and the oxygen-containing functional groups [43]. KOH addition, meanwhile, also increased nitrogen content, with a value of 10.4 wt.% observed for BC-0.1-N. As the proportion of KOH increased, the nitrogen content increased significantly and oxygen content decreased accordingly on the surface. Overall, carbon content decreased with the addition of both NH_3 and KOH, an effect that is consistent with Reactions (2) and (3).

The typical XPS spectrum for the nitrogen-doped bio-chars are provided in Figs. 5 and S2, with the typical structure of nitrogen-containing functional groups. The N 1s spectra can be deconvoluted into four peaks, specifically pyridinic-*N* (N-1, 398.2 eV), pyrrolic/pyridone-*N* (N-2, 399.8 eV), quaternary-*N* (N-3, 400.9 eV), and pyridone-*N*-oxide (N-4, 403.2 eV) [16,44,45]. Meanwhile, the relative content of these functional groups is shown in Table 4. Pyridinic-*N* and pyrrolic/pyridone-*N* are more dominant overall, which is especially beneficial given that these two functional groups are helpful in generating pseudo-capacitive behavior for supercapacitors [44,45]. These functional groups might result from NH_3 reacting with hydroxyls and carboxyls, while quaternary-*N* might result from the transformation of pyridinic-*N* into a graphitic substrate [39,46]. The addition of KOH increased the presence of pyrrolic/pyridone-*N* and pyridone-*N*-oxide, decreased quaternary-*N* content, and had no obvious influence over the amount of pyridinic-*N*.

4. Conclusions

Nitrogen-containing liquid compounds and nitrogen-doped bio-char materials were obtained from bamboo pyrolysis. The introduction of NH_3 generated many nitrogen-containing species while decreasing phenols and other oxygen-containing species. In addition, the S_{BET}, overall nitrogen content and the number of nitrogen-containing functional groups increased significantly. KOH addition both increased the bio-char yield and S_{BET}, yielding values as high as 1873 $m^2 g^{-1}$ for a nitrogen content of 9.1 wt.% in BC-0.4-N. In addition, the electrode materials generated from bio-char showed highly enhanced C_{spec} values, with a maximum value of 187 $F g^{-1}$. NH_3 and KOH addition also benefited H_2 formation, with H_2 content exceeding 50 vol.%.

Acknowledgements

The authors wish to express their great appreciation of the financial support from The National Basic Research Program of China (973 Program: 2013CB228102), The National Nature Science Foundation of China (51406061 and 51376076), Special fund for Agro-scientific Research in the Public Interest (201303095) and the technical support from Analytical and Testing Center in Huazhong University of Science & Technology (http://atc.hust.edu.cn).

Appendix A. Supplementary data

Supplementary data associated with this article can be found, in the online version, at http://dx.doi.org/10.1016/j.jaap.2016.05.004.

References

[1] S. Xin, H. Yang, Y. Chen, X. Wang, H. Chen, Assessment of pyrolysis polygeneration of biomass based on major components: product characterization and elucidation of degradation pathways, Fuel 113 (2013) 266–273.
[2] Y. Chen, H. Yang, X. Wang, S. Zhang, H. Chen, Biomass-based pyrolytic polygeneration system on cotton stalk pyrolysis: influence of temperature, Bioresource Technol. 107 (2012) 411–418.
[3] M.G. Adsul, M.S. Singhvi, S.A. Gaikaiwari, D.V. Gokhale, Development of biocatalysts for production of commodity chemicals from lignocellulosic biomass, Bioresource Technol. 102 (2011) 4304–4312.
[4] Y. Yanli, Z. Peidong, Z. Wenlong, T. Yongsheng, Z. Yonghong, W. Lisheng, Quantitative appraisal and potential analysis for primary biomass resources for energy utilization in China, Renew. Sustain. Energy Rev. 14 (2010) 3050–3058.
[5] K. Zhou, W. Zhou, Y. Du, X. Liu, Y. Sang, W. Li, J. Lu, H. Liu, S. Chen, High-performance supercapacitors based on nitrogen-doped porous carbon from surplus sludge, Sci. Adv. Mater. 7 (2015) 571–578.
[6] A. Marcilla, M. Leon, A. Nuria Garcia, E. Banon, P. Martinez, Upgrading of tannery wastes under fast and slow pyrolysis conditions, Ind. Eng. Chem. Res. 51 (2012) 3246–3255.
[7] Y.J. Bae, C. Ryu, J.K. Jeon, J. Park, D.J. Suh, Y.W. Suh, D. Chang, Y.K. Park, The characteristics of bio-oil produced from the pyrolysis of three marine macroalgae, Bioresource Technol. 102 (2011) 3512–3520.
[8] X.J. Jin, M.Y. Zhang, Y. Wu, J. Zhang, J. Mu, Nitrogen-enriched waste medium density fiberboard-based activated carbons as materials for supercapacitors, Ind. Crops Prod. 43 (2013) 617–622.
[9] Z. Li, L. Zhang, B.S. Amirkhiz, X. Tan, Z. Xu, H. Wang, B.C. Olsen, C.M.B. Holt, D. Mitlin, Carbonized chicken eggshell membranes with 3D architectures as high-performance electrode materials for supercapacitors, Adv. Energy Mater. 2 (2012) 431–437.
[10] W. Luo, B. Wang, C.G. Heron, M.J. Allen, J. Morre, C.S. Maier, W.F. Stickle, X. Ji, Pyrolysis of cellulose under ammonia leads to nitrogen-doped nanoporous carbon generated through methane formation, Nano Lett. 14 (2014) 2225–2229.
[11] N. Ferrera-Lorenzo, E. Fuente, J.M. Bermúdez, I. Suárez-Ruiz, B. Ruiz, Conventional and microwave pyrolysis of a macroalgae waste from the Agar–Agar industry. Prospects for bio-fuel production, Bioresource Technol. 151 (2014) 199–206.
[12] K. Wang, N. Zhao, S. Lei, R. Yan, X. Tian, J. Wang, Y. Song, D. Xu, Q. Guo, L. Liu, Promising biomass-based activated carbons derived from willow catkins for high performance supercapacitors, Electrochim. Acta 166 (2015) 1–11.
[13] L. Wei, H. Yang, B. Li, X. Wei, L. Chen, J. Shao, H. Chen, Absorption-enhanced steam gasification of biomass for hydrogen production: effect of calcium oxide addition on steam gasification of pyrolytic volatiles, Int. J. Hydrogen Energy 39 (2014) 15416–15423.
[14] L. Xu, Y. Jiang, Q. Yao, Z. Han, Y. Zhang, Y. Fu, Q. Guo, G.W. Huber, Direct production of indoles via thermo-catalytic conversion of bio-derived furans with ammonia over zeolites, Green Chem. 17 (2015) 1281–1290.
[15] M. Zhou, F. Pu, Z. Wang, S.Y. Guan, Nitrogen-doped porous carbons through KOH activation with superior performance in supercapacitors, Carbon 68 (2014) 185–194.
[16] L. Sun, C.G. Tian, Y. Fu, Y. Yang, J. Yin, L. Wang, H.G. Fu, Nitrogen-doped porous graphitic carbon as an excellent electrode material for advanced supercapacitors, Chem. A Eur. J. 20 (2014) 564–574.
[17] G. Wang, J. Zhang, S. Kuang, J. Zhou, W. Xing, S. Zhuo, Nitrogen-doped hierarchical porous carbon as an efficient electrode material for supercapacitors, Electrochim. Acta 153 (2015) 273–279.
[18] L. Sun, C.L. Wang, Y. Zhou, Q. Zhao, X. Zhang, J.S. Qiu, Activated nitrogen-doped carbons from polyvinyl chloride for high-performance electrochemical capacitors, J. Solid State Electrochem. 18 (2014) 49–58.
[19] Y. Gao, L. Li, Y. Jin, Y. Wang, C. Yuan, Y. Wei, G. Chen, J. Ge, H. Lu, Porous carbon made from rice husk as electrode material for electrochemical double layer capacitor, Appl. Energy 153 (2015) 41–47.
[20] H. Yang, R. Yan, H. Chen, D.H. Lee, D.T. Liang, C. Zheng, Mechanism of palm oil waste pyrolysis in a packed bed, Energy Fuels 20 (2006) 1321–1328.
[21] C. Gai, Y. Dong, Experimental study on non-woody biomass gasification in a downdraft gasifier, Int. J. Hydrogen Energy 37 (2012) 4935–4944.
[22] C.A. Alves, C. Gonçalves, C.A. Pio, F. Mirante, A. Caseiro, L. Tarelho, M.C. Freitas, D.X. Viegas, Smoke emissions from biomass burning in a Mediterranean shrubland, Atmos. Environ. 44 (2010) 3024–3033.
[23] P. Fu, S. Hu, J. Xiang, P. Li, D. Huang, L. Jiang, A. Zhang, J. Zhang, FTIR study of pyrolysis products evolving from typical agricultural residues, J. Anal. Appl. Pyrolysis 88 (2010) 117–123.
[24] R.J.M. Westerhof, D.W.F. Brilman, W.P.M. van Swaaij, S.R.A. Kersten, Effect of temperature in fluidized bed fast pyrolysis of biomass: oil quality assessment in test units, Ind. Eng. Chem. Res. 49 (2010) 1160–1168.
[25] R.J.M. Westerhof, H.S. Nygård, W.P.M. van Swaaij, S.R.A. Kersten, D.W.F. Brilman, Effect of particle geometry and microstructure on fast pyrolysis of beech wood, Energy Fuels 26 (2012) 2274–2280.
[26] H. Yang, R. Yan, H. Chen, D.H. Lee, D.T. Liang, C. Zheng, Pyrolysis of palm oil wastes for enhanced production of hydrogen rich gases, Fuel Process. Technol. 87 (2006) 935–942.
[27] H.P. Boehm, G. Mair, T. Stoehr, A.R. De Rincón, B. Tereczki, Carbon as a catalyst in oxidation reactions and hydrogen halide elimination reactions, Fuel 63 (1984) 1061–1063.
[28] B. Stöhr, H.P. Boehm, R. Schlögl, Enhancement of the catalytic activity of activated carbons in oxidation reactions by thermal treatment with ammonia or hydrogen cyanide and observation of a superoxide species as a possible intermediate, Carbon 29 (1991) 707–720.
[29] L. Moens, R.J. Evans, M.J. Looker, M.R. Nimlos, A comparison of the Maillard reactivity of proline to other amino acids using pyrolysis-molecular beam mass spectrometry, Fuel 83 (2004) 1433–1443.
[30] M.A. Lillo-Ródenas, J. Juan-Juan, D. Cazorla-Amorós, A. Linares-Solano, About reactions occurring during chemical activation with hydroxides, Carbon 42 (2004) 1371–1375.
[31] V. Jiménez, P. Sánchez, J.L. Valverde, A. Romero, Influence of the activating agent and the inert gas (type and flow) used in an activation process for the porosity development of carbon nanofibers, J. Colloid Interface Sci. 336 (2009) 712–722.
[32] H. Deng, G. Li, H. Yang, J. Tang, J. Tang, Preparation of activated carbons from cotton stalk by microwave assisted KOH and K_2CO_3 activation, Chem. Eng. J. 163 (2010) 373–381.
[33] J. Liu, X. Jiang, J. Shen, H. Zhang, Pyrolysis of superfine pulverized coal. Part 3. Mechanisms of nitrogen-containing species formation, Energy Convers. Manage. 94 (2015) 130–138.
[34] T.V.W. Janssens, H. Falsig, L.F. Lundegaard, P.N.R. Vennestrøm, S.B. Rasmussen, P.G. Moses, F. Giordanino, E. Borfecchia, K.A. Lomachenko, C. Lamberti, S. Bordiga, A. Godiksen, S. Mossin, P. Beato, A consistent reaction scheme for the selective catalytic reduction of nitrogen oxides with ammonia, ACS Catal. 5 (2015) 2832–2845.
[35] J.E. Hodge, Dehydrated foods, chemistry of browning reactions in model systems, J. Agric. Food Chem. 1 (1953) 928–943.
[36] C.L. Mangun, K.R. Benak, J. Economy, K.L. Foster, Surface chemistry, pore sizes and adsorption properties of activated carbon fibers and precursors treated with ammonia, Carbon 39 (2001) 1809–1820.
[37] D. Lozano-Castelló, M.A. Lillo-Ródenas, D. Cazorla-Amorós, A. Linares-Solano, Preparation of activated carbons from Spanish anthracite: I. Activation by KOH, Carbon 39 (2001) 741–749.
[38] X.Y. Chen, C. Chen, Z.J. Zhang, D.H. Xie, X. Deng, J.W. Liu, Nitrogen-doped porous carbon for supercapacitor with long-term electrochemical stability, J. Power Sources 230 (2013) 50–58.
[39] H.B. Zhao, W.D. Wang, Q.F. Lü, T.T. Lin, Q. Lin, H. Yang, Preparation and application of porous nitrogen-doped graphene obtained by co-pyrolysis of lignosulfonate and graphene oxide, Bioresource Technol. 176 (2015) 106–111.
[40] X.Q. Wang, C.G. Liu, D. Neff, P.F. Fulvio, R.T. Mayes, A. Zhamu, Q. Fang, G.R. Chen, H.M. Meyer, B.Z. Jang, S. Dai, Nitrogen-enriched ordered mesoporous carbons through direct pyrolysis in ammonia with enhanced capacitive performance, J. Mater. Chem. A 1 (2013) 7920–7926.

[41] Y. Gao, W. Zhang, Q. Yue, B. Gao, Y. Sun, J. Kong, P. Zhao, Simple synthesis of hierarchical porous carbon from Enteromorpha prolifera by a self-template method for supercapacitor electrodes, J. Power Sources 270 (2014) 403–410.
[42] D. Saha, Y. Li, Z. Bi, J. Chen, J.K. Keum, D.K. Hensley, H.A. Grappe, H.M. Meyer III, S. Dai, M.P. Paranthaman, A.K. Naskar, Studies on supercapacitor electrode material from activated lignin-derived mesoporous carbon, Langmuir 30 (2014) 900–910.
[43] D. Hulicova-Jurcakova, M. Kodama, S. Shiraishi, H. Hatori, Z.H. Zhu, G.Q. Lu, Nitrogen-enriched nonporous carbon electrodes with extraordinary supercapacitance, Adv. Funct. Mater. 19 (2009) 1800–1809.
[44] B. Xu, S. Hou, G. Cao, F. Wu, Y. Yang, Sustainable nitrogen-doped porous carbon with high surface areas prepared from gelatin for supercapacitors, J. Mater. Chem. 22 (2012) 19088–19093.
[45] D. Hulicova-Jurcakova, M. Seredych, G.Q. Lu, T.J. Bandosz, Combined effect of nitrogen- and oxygen-containing functional groups of microporous activated carbon on its electrochemical performance in supercapacitors, Adv. Funct. Mater. 19 (2009) 438–447.
[46] Z. Lin, G. Waller, Y. Liu, M. Liu, C.P. Wong, Facile synthesis of nitrogen-doped graphene via pyrolysis of graphene oxide and urea, and its electrocatalytic activity toward the oxygen-reduction reaction, Adv. Energy Mater. 2 (2012) 884–888.